

DINO-Tok: Adapting DINO for Visual Tokenizers

Mingkai Jia^{1,2} Mingxiao Li² Zhijian Shu^{2,3} Anlin Zheng⁴
Liaoyuan Fan² Jiaxin Guo⁵ Tianxing Shi³ Dongyue Lu² Zeming Li¹
Xiaoyang Guo² Xiaojuan Qi⁴ Xiao-Xiao Long³ Qian Zhang²
Ping Tan^{1*} Wei Yin^{2**}

¹The Hong Kong University of Science and Technology ²Horizon Robotics
³Nanjing University ⁴Hong Kong University
⁵The Chinese University of Hong Kong

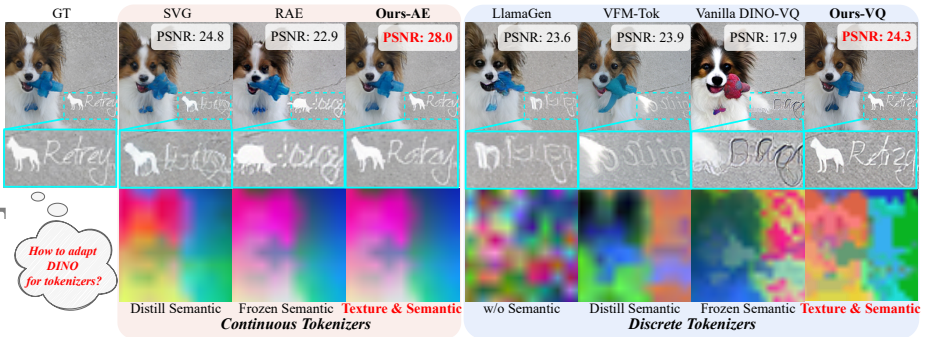


Fig. 1: How to Adapt DINO for Visual Tokenizers? (Top): RGB reconstructions. Distilling or freezing DINO features exposes the texture–semantic trade-off such as color shifts and high-dimensional quantization instability or semantic replacement, while DINO-Tok-AE and DINO-Tok-VQ recover fine texture details and correct semantics. **(Bottom): PCA of latent features.** DINO-Tok produces a more structured semantic latent space, whereas distilled or frozen tokenizers yield noisier ones.

Abstract. Recent advances in visual generation have emphasized the importance of Latent Generative Models (LGMs), which critically depend on effective visual tokenizers to bridge pixels and semantic representations. However, tokenizers constructed on pre-trained vision foundation models (VFMs) often struggle to balance semantic richness and reconstruction fidelity in high-dimensional latent spaces. In this paper, we introduce **DINO-Tok**, a visual tokenizer built upon a frozen DINO encoder that supports both continuous autoencoding (**DINO-Tok-AE**) and discrete vector-quantization (**DINO-Tok-VQ**). By unifying hierarchical representations from both shallow fine-grained features and deep global semantics into an information-complete latent space, DINO-Tok preserves *texture details* while maintaining *semantic consistency* for generation. We further investigate VQ in frozen semantic feature spaces of high dimensionality, where information dilution and codebook collapse frequently arise. To address this issue, we propose **Dominant-Subspace Quantization (DSQ)**, which leverages a global PCA analysis to select

* Co-corresponding Author.

** Co-corresponding Author. Project Leader.

principal components while suppressing noisy dimensions, thereby stabilizing codebook optimization and improving reconstruction and generation quality. On ImageNet 256×256 , DINO-Tok achieves strong reconstruction performance, achieving **0.28** rFID for continuous autoencoding and **1.10** rFID for discrete VQ, as well as strong few-step generation performance **1.82** gFID for diffusion and **2.44** gFID for autoregressive generation. These results demonstrate that pre-trained VFMs such as DINO can be directly adapted into high-fidelity, semantically aligned visual tokenizers for next-generation latent generative models.

1 Introduction

Recent advances in large-scale generative models have demonstrated the power of high-level representation learning across vision and language [4, 23, 52]. In the visual domain, most generative models [8, 36] critically rely on visual tokenizers that convert raw pixels into compact latent features. However, existing tokenizers, including variational autoencoders (VAEs) [19], vector quantized variational autoencoders (VQ-VAEs) [14, 45], and their recent variants [9, 30, 37, 43, 53, 57, 62], are primarily optimized for reconstruction fidelity rather than semantic representation. Consequently, the learned latent spaces are often low-dimensional, task-specific, and lack structural alignment with high-level semantics, limiting their expressiveness in modern generative modeling.

In parallel, pretrained vision foundation models (VFMs) such as DINO [7, 31, 40] have demonstrated strong capabilities in extracting semantically structured and generalizable features. Recent works [52, 59] distill VFM [31, 34, 40, 44] knowledge into tokenizers to improve semantic alignment, while RAE [60] directly utilizes a frozen VFM as the encoder and observes clear gains in image generation. However, whether through distillation or direct usage, leveraging VFM features for tokenization still faces two key challenges: (1) **Texture-semantic trade-off**: Deep VFM layers capture global semantics but the features lack low-level texture information, leading to color shifts, missing fine details, and low PSNR, as depicted in Fig. 1, 2, and 4; (2) **High-dimensional quantization instability**: Tokenizers designed for continuous diffusion models cannot be directly converted into discrete tokenizers for autoregressive generation. *e.g.*, directly discretizing high-dimensional frozen VFM features often triggers codebook collapse and semantic replacement, as described in Fig. 1, 4. These observations motivate a natural question: *Could a pretrained representation model, such as DINO, be directly adapted into an effective unified visual tokenizer for both continuous and discrete generative modeling?*

To answer this question, we propose **DINO-Tok**, a representation-driven hybrid tokenizer built on a frozen DINO encoder, comprising a continuous tokenizer DINO-Tok-AE and a discrete tokenizer DINO-Tok-VQ. To resolve the texture-semantic trade-off, DINO-Tok-AE constructs an **information-complete latent space** by integrating fine-grained detail features from shallow layers with deep global semantics, preserving high-frequency textures while maintaining semantic consistency. The specified shallow layer could both provide rich high-

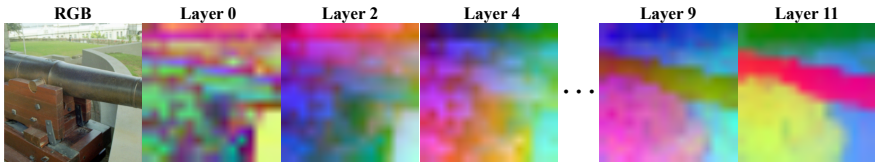


Fig. 2: PCA visualizations across shallow to deep layers of DINO-base. As depth increases, DINO features become more semantically clustered, while fine-grained details fade, indicating increasingly structured representations.

frequency details to complement semantics and remain sufficiently structured to align with frozen DINO features without additional distillation. Our layer-wise analysis (see Fig. 8) shows that an intermediate shallow layer best satisfies this trade-off, yielding the most favorable balance between reconstruction quality and generative performance.

For discrete modeling, discretizing such frozen, high-dimensional semantic spaces introduces additional difficulty for VQ. To address this issue, we introduce **Dominant-Subspace Quantization (DSQ)** in DINO-Tok-VQ. Guided by a global PCA analysis of DINO features, DSQ selects a principal semantic component subspace and performs VQ only along these principal directions while suppressing noisy, low-variance dimensions. This design maintains the effective dimensions to address the quantization problem, restores the discriminative power of distance, and stabilizes codebook optimization, yielding discrete tokens that remain semantically consistent with the underlying frozen VFM.

This representation-driven design delivers strong empirical performance: DINO-Tok achieves state-of-the-art reconstruction on ImageNet 256×256 (0.28 rFID for AE, 1.10 rFID for VQ) and superior generative quality (few-step 1.82 gFID for diffusion and 2.44 gFID for AR) compared to existing methods under identical settings. Our contributions are threefold:

- We analyze the challenges of adapting the frozen DINO to vision tokenizers, identifying texture-semantic trade-off and quantization instability in high-dimensional semantic spaces.
- We propose **DINO-Tok-AE**, a continuous tokenizer that fuses hierarchical DINO features into an **information-complete latent space**, achieving high-fidelity reconstruction while preserving semantic structure.
- We introduce **DINO-Tok-VQ** with **dominant-subspace quantization**, which quantizes principal dimensions of frozen DINO features, leading to stable, semantically consistent discrete tokens and improved reconstruction and generation performance.

2 Related Works

Continuous Visual Tokenizers. Continuous visual tokenizers, often based on variational autoencoders (VAEs) [19], map pixel-level inputs into continuous

latent spaces, enabling efficient training of latent diffusion models [10, 12, 25, 35, 36, 49] with high-fidelity reconstruction.

Recent efforts [52, 55, 60] have focused on improving the semantic structure of the latent space by leveraging pretrained VFMs [16, 20, 31, 34]. REPA [55] aligns DiT middle block features with representations. VA-VAE [52] further introduces semantic supervision via latent-space distillation, encouraging disentangled and meaningful representations. Although generation quality improves, weak supervision constrains semantic information retention. RAE [60] takes a more direct approach by replacing the VAE encoder with a frozen vision backbone, aiming at stronger semantic priors. This setup enhances representational understanding but struggles with fine details and color accuracy. It often produces outputs resembling semantic substitutions rather than faithful reconstructions. To overcome this texture–semantic trade-off, we propose a dual-branch tokenizer, named DINO-Tok that fuses DINO’s last-layer features for semantic content and early-layer features for structural details. This design improves both reconstruction and semantic, leading to a balanced and effective continuous latent space.

Discrete Visual Tokenizers. Discrete visual tokenizers, typically implemented as VQ-VAEs [14, 38, 46, 48, 50, 56, 58], encode image features into discrete codes by looking up the nearest entries in a learnable codebook. The discrete tokens enable the ability for autoregressive approaches with efficient storage and compatibility with vision language models (VLMs) and world models (WMs) [1, 17, 21]. However, recent works such as LlamaGen [41] and Emu3 [47] observe that high-dimensional latents severely degrade quantization, leading to poor reconstruction quality and underutilized codebooks. As a result, these models reduce the bottleneck dimension to 8 to stabilize training.

While this low-dimensional latent improves quantization behavior, it introduces significant information loss during compression. To alleviate this, recent methods [27, 30, 53] adopt lookup-free quantization, directly projecting features into fixed discrete codebook vectors without nearest-neighbor search. Others [3, 5, 24, 54, 59] follow a different path by distilling visual foundation model features into the discrete latent space. Despite this semantic alignment, they both constrain the latent dimensionality (e.g., LFQ [27] uses a binary codebook of size 2^{18} with a bottleneck dimension of 18), which limits representational capacity. Some methods [18, 22, 28, 42, 64] address this by splitting the latent vector into multiple low-dimensional subspaces, each quantized separately. While effective for maintaining quantization quality, such low per-channel dimensions limit the utilization of high-dimensional semantic information.

In contrast, DINO-Tok starts from the full 768-dimensional latent space of DINO’s final layer and applies DSQ, which leverages a global PCA analysis to select a principal semantic latent subspace and performs quantization only along these directions, enabling stable and meaningful codebook learning, which overcomes the inherent difficulty of optimizing codebooks in frozen high-dimensional semantic spaces while preserving fine-grained, structured visual information.

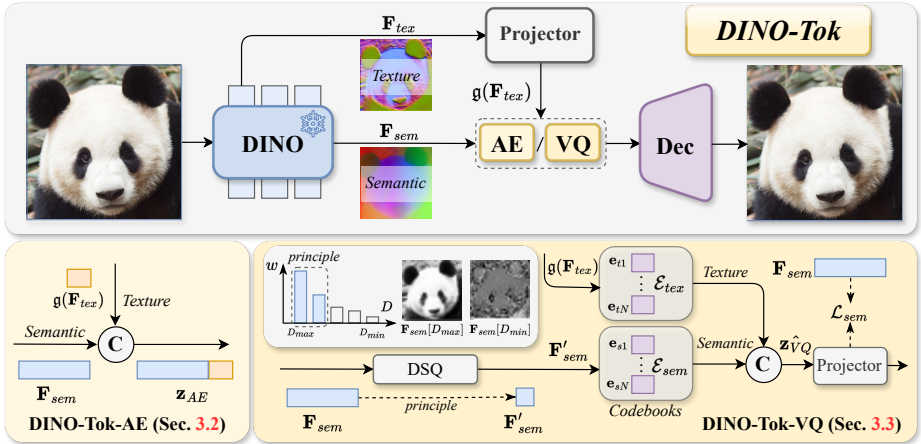


Fig. 3: DINO-Tok framework. We adapt a frozen DINO encoder into a unified visual tokenizer for both continuous and discrete generative modeling. **DINO-Tok-AE** forms an **information-complete latent** by concatenating deep semantics with a projected shallow feature to improve reconstruction fidelity. **DINO-Tok-VQ** discretizes this representation with **DSQ** and two specialized codebooks for semantics and texture to stabilize high-dimensional lookup while preserving fine details. We further apply an additional semantic alignment loss to retain high-level semantics while maintaining reconstructive quality.

3 DINO-Tok: Adapting DINO for Unified Tokenization

Recent works [28, 52, 59] have demonstrated that incorporating pretrained VFMs into visual tokenizers, either via distillation [39, 59] or directly using them as frozen encoders [60], can accelerate convergence and improve generative quality. However, distillation typically transfers only a portion of the semantic structure, while directly using frozen VFM features exposes two fundamental challenges:

- **Texture–semantic trade-off.** Deep VFM features are highly semantic, but lack detailed information such as color and textures that are crucial for high-fidelity reconstruction.
- **Quantization instability in frozen high-dimensional semantic spaces.** Directly applying VQ to frozen high-dimensional features (e.g., $d = 768$ for DINO-Base) suffers from distance measurement failure and semantic imbalance across channels, leading to codebook collapse and semantic replacement.

These two challenges lead to the central problem posed in the introduction: *could the frozen representation models be encoders for both continuous and discrete tokenizers?* To this end, we design **DINO-Tok**, a representation-driven hybrid tokenizer built on a frozen DINO [40] encoder. It comprises a continuous tokenizer, **DINO-Tok-AE**, which constructs an information-complete latent by fusing shallow texture features with deep semantic features to resolve the texture–semantic trade-off, and a discrete tokenizer, **DINO-Tok-VQ**, which

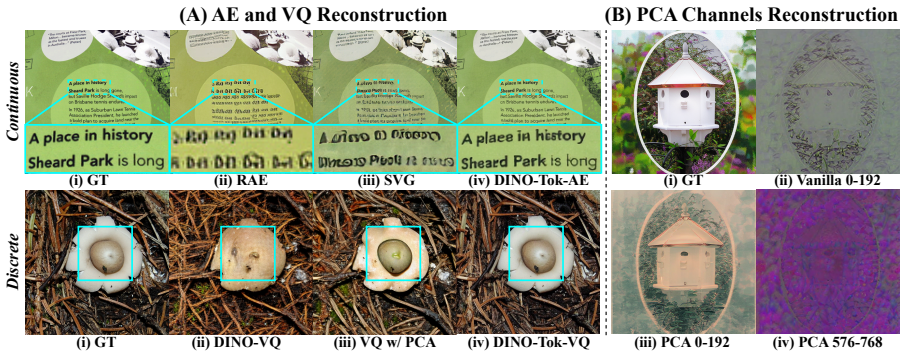


Fig. 4: (Left): DINO-based AE/VQ reconstructions. *Top: continuous.* DINO-Tok-AE restores textures and colors via dual-branch features. *Bottom: discrete.* Vanilla VQ suffers from semantic replacement and overlap, our dual-branch design with PCA-based VQ achieves faithful reconstruction. **(Right): Channel ablation on DINO.** Top-192 PCA-ranked channels (iii) preserve object semantics and structure better than the first 192 raw channels (ii), while the lowest-192 channels (iv) collapse to blurry noise, showing that informative content concentrates in high-eigenvalue components.

applies DSQ to stabilize VQ in frozen high-dimensional semantic spaces by quantizing principle components while preserving critical semantic information.

The overview is illustrated in Fig. 3. DINO-Tok-AE and DINO-Tok-VQ shared the same backbone, and we first train AE, then discretize the same fused latent using DSQ. The method section is organized as follows: Sec. 3.1 analyzes the detailed challenges of frozen DINO tokenization. Sec. 3.2 describes how we design our fused multi-layer dual-branch autoencoder upon frozen VFM DINOv3 [40]. Sec. 3.3 shows the DSQ design and dual codebooks following our AE. Sec. 3.4 presents our generative model design.

3.1 Challenges of Frozen DINO Tokenization

Texture–semantic trade-off. A straightforward baseline, as in RAE [60], is to pair a trainable decoder with a frozen DINO encoder and decode directly from the final-layer feature F_{sem} . However, Fig. 1 and 4 show that reconstructions suffer from color shifts, missing high-frequency textures, and low PSNR. This degradation indicates that F_{sem} is *information-incomplete*: DINO is optimized for semantic structural latent space, suppressing low-level appearance variations that are essential for pixel-level fidelity. Prior work such as SVG [39] partially alleviates this by introducing an extra residual encoder to recover fine details from pixels, but the underlying texture–semantic trade-off remains.

High-Dimensional Quantization Instability. Extending a pretrained visual foundation model to build a discrete tokenizer [45] introduces further complications. As dimensionality increases, pairwise distances tend to concentrate [6]: the ratio between nearest and farthest neighbor distances approaches 1, making L_2 -based nearest-neighbor assignments numerically indistinguishable. See supplementary materials for detailed analysis. In frozen DINO semantic spaces,

this distance concentration leads to eventual codebook collapse (See Tab. 3), together with semantic replacement artifacts (See Fig. 4) in the reconstructed images. Meanwhile, a global PCA analysis on DINO features (Fig. 5) and vanilla DINO PCA channels reconstructions (Fig. 4-(B)) reveal a pronounced semantic imbalance across channels: a small set of principal components captures coherent semantic and spatial structure, while many tail dimensions are low-variance and noisy. Uniform quantization over all channels therefore dilutes dominant semantic components and wastes capacity on noisy dimensions, further aggravating quantization instability in frozen high-dimensional semantic spaces. Existing approaches [41, 47] typically utilize very low-dimensional codebooks (e.g., 8 channels) to mitigate codebook collapse, but such aggressive compression sacrifices latent information capacity. High-dimensional VQ methods [38, 63] rely on jointly optimizing all codes simultaneously, and thus are hard to align with frozen encoded semantic features, whose structural latent space we aim to preserve. These limitations motivate our *dominant-subspace* view of quantization.

3.2 DINO-Tok-AE: Information-complete Latents

To resolve the **texture–semantic trade-off** of the frozen DINO features, DINO-Tok-AE constructs an *information-complete* dual-branch latent that explicitly fuses deep semantic features with shallow texture features which are necessary for faithful reconstruction. (See Fig. 2.)

Let a frozen DINO encoder extract hierarchical features $\{\mathbf{F}_l\}_{l=1}^L$ from an input image $\mathbf{x} \in \mathbb{R}^{H \times W \times 3}$, where $\mathbf{F}_l \in \mathbb{R}^{H_l \times W_l \times C_l}$ is the feature map at layer l . Denote the final-layer feature as \mathbf{F}_{sem} and a selected shallow-layer feature as \mathbf{F}_{tex} . We first project the texture feature into a compact embedding using a lightweight projector $\mathbf{g}(\cdot)$, and then build the **information-complete latent** by channel-wise concatenation: $\mathbf{z}_{AE} = [\mathbf{F}_{sem}; \mathbf{g}(\mathbf{F}_{tex})]$, where $[\cdot; \cdot]$ denotes concatenation. Intuitively, \mathbf{F}_{sem} anchors global semantics and layout, while $\mathbf{g}(\mathbf{F}_{tex})$ injects fine-grained texture details that are suppressed by semantic latents.

We decode \mathbf{z}_{AE} with a trainable decoder D_{AE} to reconstruct the image: $\hat{\mathbf{x}}_{AE} = D(\mathbf{z}_{AE})$, and optimize D_{AE} with traditional reconstruction loss \mathcal{L}_{rec} , perceptual loss \mathcal{L}_{perc} and GAN loss \mathcal{L}_{GAN} following VQGAN [14], denoted as:

$$\mathcal{L}_{AE} = \lambda_{rec}\mathcal{L}_{rec} + \lambda_{perc}\mathcal{L}_{perc} + \lambda_{GAN}\mathcal{L}_{GAN}, \quad (1)$$

and the DINO [40] encoder is kept frozen. The dual-branch design reduces inversion difficulty by enabling direct use of explicit texture cues from \mathbf{F}_{tex} , rather than recovering fine-grained textures from semantic features alone. The resulting continuous latent \mathbf{z}_{AE} thus becomes both semantically structured and texture-complete, forming a strong basis for subsequent discretization.

3.3 DINO-Tok-VQ: Dominant-Subspace Quantization

We build DINO-Tok-VQ by discretizing the fused dual-branch latent while respecting the structure of frozen DINO features. Since direct VQ on the high-dimensional space with L_2 distance is challenging due to distance concentration

and semantic imbalance, we propose **DSQ**, which performs VQ in a principal semantic latent subspace rather than in the full high-dimensional space.

Global PCA on frozen DINO features. We first perform a global PCA on \mathbf{F}_{sem} computed over a large ImageNet subset offline. Let $\mathbf{P} \in \mathbb{R}^{C_{sem} \times k}$ be the projection matrix formed by the top- k eigenvectors ($k \ll C_{sem}$). For each token i , we obtain the projected semantic feature $\mathbf{F}'_{sem}{}^{(i)}$. This projection selects a *principle semantic latent subspace* where most semantic structure is concentrated in these dimensions, while many noisy, low-variance channels are discarded. (See Fig. 5.) Reducing dimensionality in this way mitigates distance concentration for VQ while preserving critical semantic information.

Dual-branch codebooks. Attaining the dual branch design of DINO-Tok-AE, we maintain two codebooks, including a semantic codebook $\mathcal{E}_{sem} = \mathbf{e}_{sk}$, $k = 1, \dots, N$ operating in the dominant semantic subspace, and a texture codebook $\mathcal{E}_{tex} = \mathbf{e}_{tk}$, $k = 1, \dots, N$ operating on the projected texture embeddings with codebook size N . For each token i , we quantize by:

$$\mathbf{q}_{sem}^{(i)} = \arg \min_{\mathbf{e}_{sk} \in \mathcal{E}_{sem}} \|(\mathbf{F}'_{sem}{}^{(i)} - \mathbf{e}_{sk})\|_2^2, \quad \mathbf{q}_{tex}^{(i)} = \arg \min_{\mathbf{e}_{tk} \in \mathcal{E}_{tex}} \|(\mathbf{F}'_{tex}{}^{(i)} - \mathbf{e}_{tk})\|_2^2. \quad (2)$$

The resulting quantized latent at location i is then: $\hat{\mathbf{z}}_{VQ}^{(i)} = [\mathbf{q}_{sem}^{(i)}, \mathbf{q}_{tex}^{(i)}]$, and the full latent $\hat{\mathbf{z}}_{VQ}$ is projected back to the high dimension by $\mathbf{g}_\theta(\hat{\mathbf{z}}_{VQ})$ and then fed to the decoder D to obtain the reconstructed image $\hat{\mathbf{x}}_{VQ} = D(\mathbf{g}_\theta(\hat{\mathbf{z}}_{VQ}))$.

Semantic consistency regularization. To ensure that discretization does not distort the frozen semantic structure, we add a semantic alignment loss. A small projector $\mathbf{g}_\theta(\cdot)$ maps $\hat{\mathbf{z}}_{VQ}$ back to the original high-dimensional semantic space, and we penalize deviation from \mathbf{F}_{sem} via cosine similarity by $\mathcal{L}_{sem} = 1 - \cos(\mathbf{g}_\theta(\hat{\mathbf{z}}_{VQ}), \mathbf{F}_{sem})$. This term regularizes token alignment with the frozen DINO semantics, enhancing semantic structure under DSQ.

Training objective. Following VQGAN [14], we use codebook and commitment losses \mathcal{L}_{VQ} in addition to \mathcal{L}_{AE} and \mathcal{L}_{sem} :

$$\mathcal{L} = \mathcal{L}_{AE} + \mathcal{L}_{VQ} + \mathcal{L}_{sem}. \quad (3)$$

We keep the DINO encoder frozen and optimize codebooks, projector heads, and the decoder. DSQ thus stabilizes VQ in frozen high-dimensional semantic spaces by (i) quantizing in a principle semantic latent subspace and (ii) enforcing semantic consistency to the original DINO features.

3.4 Image Generation with DINO-Tok

To assess the usefulness of DINO-Tok for downstream generation, we plug it into two representative generative paradigms: *continuous-space generation* operating on *continuous* latents and *discrete generation* operating on *discrete* tokens. Concretely, we follow the generation setups of VAVAE [52] for diffusion and LlamaGen [41] for autoregressive modeling, while replacing their tokenizers with our DINO-Tok-AE and DINO-Tok-VQ, respectively.

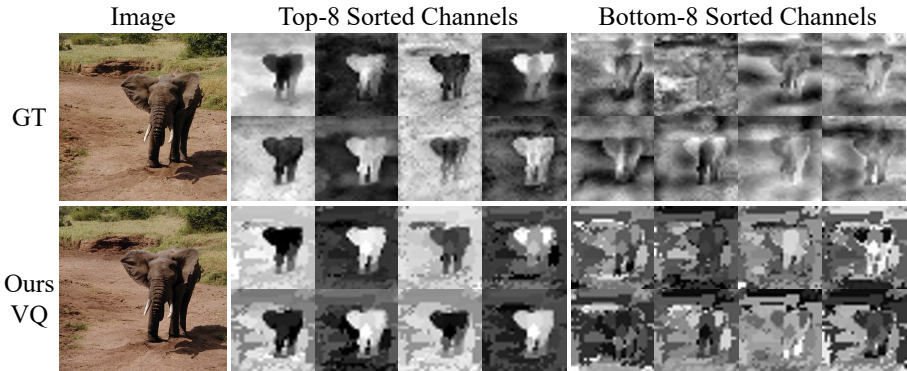


Fig. 5: Visualization of PCA-sorted feature channels. PCA-sorted channel visualization. Channels are ordered by global PCA eigenvalues. High-ranked channels capture clear spatial structures, while low-ranked ones are noisy. Our PCA-guided VQ stabilizes quantization and improves reconstruction fidelity.

Continuous-space generation with DINO-Tok-AE. For continuous-space generation, an image is encoded by our fused multi-layer dual-branch tokenizer into the texture-augmented semantic latent $\mathbf{z}_{\text{AE}} = [\mathbf{F}_{\text{sem}}; \mathbf{g}(\mathbf{F}_{\text{tex}})]$, which is decoded to pixels by D . We then train a latent generator G_{AE} to model the distribution of \mathbf{z}_{AE} . Since \mathbf{z}_{AE} consists of a semantic branch and a texture branch, we compute the latent objective separately on the two channel subsets and average them: $\mathcal{L}_{\text{latent}} = \frac{1}{2}(\mathcal{L}_{\text{latent}}^{\text{sem}} + \mathcal{L}_{\text{latent}}^{\text{tex}})$, which encourages balanced modeling of both semantics and textures rather than collapsing to a single branch. At sampling time, G_{AE} produces a latent $\tilde{\mathbf{z}}_{\text{AE}}$ in the same space, which is rendered into the final image by D .

Discrete-token generation (DINO-Tok-VQ). For discrete-token generation, each spatial location is mapped to two sub-codes by our dual-codebook quantization, one from the semantic codebook \mathcal{E}_{sem} and the other from the texture codebook \mathcal{E}_{tex} . We adopt the transformer backbone of LlamaGen [41] as a discrete generator G_{disc} and adapt its output layer to our two-codebook setting. The shared backbone produces a hidden state $h^{(i)}$ at each token position, which is fed into two separate linear heads to predict logits for the semantic and texture codebooks respectively, $\ell_{\text{sem}}^{(i)} = W_{\text{sem}}h^{(i)}$, $\ell_{\text{tex}}^{(i)} = W_{\text{tex}}h^{(i)}$. The training loss is the sum of two cross-entropy terms, $\mathcal{L}_{\text{disc}} = \mathcal{L}_{\text{CE}}(\ell_{\text{sem}}, \mathbf{y}_{\text{sem}}) + \mathcal{L}_{\text{CE}}(\ell_{\text{tex}}, \mathbf{y}_{\text{tex}})$, where \mathbf{y}_{sem} and \mathbf{y}_{tex} are ground-truth semantic and texture code indices produced by DINO-Tok-VQ. At inference time, G_{VQ} autoregressively generates both sub-codes at each position, which are then mapped back by \mathcal{E}_{sem} and \mathcal{E}_{tex} , concatenated into $\hat{\mathbf{z}}_{\text{VQ}}$, and finally decoded into pixels by the shared decoder D .

Table 1: Comparative evaluation of DINO-Tok-AE on ImageNet-1k 256×256 reconstruction and class-conditional generation. DINO-Tok-AE is trained only on ImageNet-1k and achieves notable reconstruction performance. For generation, DINO-Tok-AE-XL benefits from larger latent dimensions, reaching competitive performance with only 80 training epochs and 25 sampling steps. * denotes results without classifier-free guidance (CFG).

Method	Reconstruction		Generation					
	Tokenizer	rFID↓	#Epoch	#Step	gFID*↓	IS*↑	gFID↓	IS↑
MaskDiT-XL [61]	SD-VAE	0.87	1600	250	5.69	177.9	2.28	276.6
DiT-XL [32]	SD-VAE	0.87	1600	250	9.62	121.5	2.27	278.2
SiT-XL [29]	SD-VAE	0.87	1600	250	8.61	131.7	2.06	270.3
Faster-DiT [51]	SD-VAE	0.87	400	250	7.91	131.3	2.03	264.0
MDT [15]	SD-VAE	0.87	1300	250	6.23	143.0	1.79	283.0
REPA-XL [55]	SD-VAE	0.87	800	250	5.90	–	1.42	305.7
SiT-XL [55]	VA-VAE	0.28	800	250	5.96	128.0	3.63	290.6
SiT-XL [55]	VA-VAE	0.28	80	25	7.29	121.0	4.13	279.7
SVG-XL [55]	SVGTok	0.65	80	25	6.57	137.9	<u>3.54</u>	207.6
RAE-XL [60]	RAE	<u>0.49</u>	80	25	2.32	204.8	–	–
Ours-AE-XL	DINO-Tok-AE	0.28	80	25	<u>3.03</u>	<u>176.7</u>	2.27	<u>221.8</u>
SVG-XL [55]	SVGTok	0.65	500	25	3.94	169.3	2.10	258.7
SVG-XL [55]	SVGTok	0.65	1400	25	3.36	181.2	<u>1.92</u>	<u>264.9</u>
RAE-XL [60]	RAE	<u>0.49</u>	800	25	1.76	237.1	–	–
Ours-AE-XL	DINO-Tok-AE	0.28	800	25	<u>2.40</u>	<u>216.2</u>	1.82	273.7

4 Experiments

4.1 Implementation Details

Training Setup. Since the designed visual tokenizers are built upon a frozen pre-trained vision foundation model, only the parameters of newly introduced modules, including the projector, quantizer, and decoder, are learnable. We first train the autoencoders (DINO-Tok-AE), then introduce discrete quantization and finetune it to the DINO-Tok-VQ. All the training procedures employ a base learning rate of 1e-4. We use the AdamW [26] optimizer with β_1 and β_2 as 0.9 and 0.95. All models are trained on ImageNet-1k [11] training set while evaluated on the validation set with image resolution of 256×256 . Additionally, we strictly follow VAAE [52] for continuous-space generation and LlamaGen [41] for discrete-space generation, respectively.

Evaluation Setting. For image reconstruction evaluation, we employ reconstruction Fréchet Inception Distance (rFID) to measure the quality, and for image generations, we employ gFID and inception score (IS) for evaluation, following the standard protocol in prior work [29, 41, 52, 60].

4.2 Comparative Studies

Reconstruction Quality Comparison. Table 1 and Table 2 report reconstruction rFID on ImageNet-1k at 256×256 for both continuous (DINO-Tok-AE) and discrete (DINO-Tok-VQ) tokenizers. On the continuous side, DINO-

Table 2: Comparative evaluation of DINO-Tok-VQ on ImageNet-1k 256×256 reconstruction and autoregressive class-conditional generation.

Method	Reconstruction		Generation		
	Tokenizer	rFID↓	#Param.	gFID↓	IS↑
LlamaGen-L [41]	VQGAN [14]	4.98	343M	3.81	248.3
LlamaGen-L [41]	TiTok-L [54]	2.21	343M	4.03	219.5
MaskGIT [8]	MaskGiT [8]	2.28	675M	4.02	355.6
VAR-d16 [43]	VAR [43]	-	310M	3.30	274.4
VFM Tok-L [59]	VFM Tok	1.13	343M	2.75	278.8
Ours-VQ-L	DINO-Tok-VQ	1.10	343M	2.66	247.7
VQGAN [14]	VQGAN [14]	4.98	1.4B	15.78	74.3
LlamaGen-XXL [41]	VQGAN [14]	4.98	1.4B	<u>3.08</u>	<u>253.6</u>
RQ-Transformer [22]	RQ-VAE [22]	<u>3.20</u>	1.4B	8.71	-
Ours-VQ-XXL	DINO-Tok-VQ	1.10	1.4B	2.44	254.2

Tok-AE-XL attains an rFID of **0.28**, matching VA-VAE [52] (0.28 rFID) and clearly outperforming representation-based tokenizers such as RAE-XL [60] (0.49 rFID) and SVG-XL [55] (0.65 rFID), as well as SD-VAE based frameworks (0.87 rFID). This confirms that our dual-branch information-complete latent effectively resolves the texture–semantic trade-off. On the discrete side, DINO-Tok-VQ reaches an rFID of **1.10**, significantly improving over VQGAN used in LlamaGen (4.98 rFID) and also surpassing other methods, indicating that DSQ preserves critical information for reconstruction under vector quantization.

Continuous-space class-conditional generation. We next evaluate class-conditioned generation in continuous-space by plugging DINO-Tok-AE into the continuous generator (Table 1). We focus on the few-step generation with only 25 sampling steps. Under this setting and 80 epochs of training, DINO-Tok-AE-XL achieves a gFID of **2.27** with classifier-free guidance (CFG) and 3.03 without CFG, outperforming SVG-XL [39] (3.54 gFID with CFG) and VA-VAE [52] (4.13 gFID with CFG), and approaching RAE-XL [60] (2.32 gFID without CFG), while offering much stronger reconstruction (0.28 v.s. 0.49 rFID) quality and preserving the frozen semantic structure. When training is extended to 800 epochs, DINO-Tok-AE-XL further improves to a gFID of **1.82** and IS of **273.7** with 25 steps, surpassing SVG-XL [39] at the same step budget and clearly outperforming VA-VAE [52] in the few-step setting. These results show that an information-complete latent from DINO-Tok-AE not only preserves reconstruction fidelity, but also enables efficient few-step continuous-space generation with competitive or superior performance compared to prior tokenizers.

Discrete-token class-conditional generation. Finally, we assess discrete-token generation by combining DINO-Tok-VQ with the LlamaGen-style autoregressive generator (Table 2). At the L-scale (343M parameters), DINO-Tok-VQ-L attains a gFID of 2.66 and IS of 247.7 with rFID 1.10, improving gFID over LlamaGen-L (3.81 gFID, 248.3 IS) while delivering much better reconstruction and semantic fidelity. At the XXL scale (1.4B parameters), DINO-Tok-VQ-XXL achieves 2.44 gFID and 254.2 IS, outperforming the baseline LlamaGen-XXL

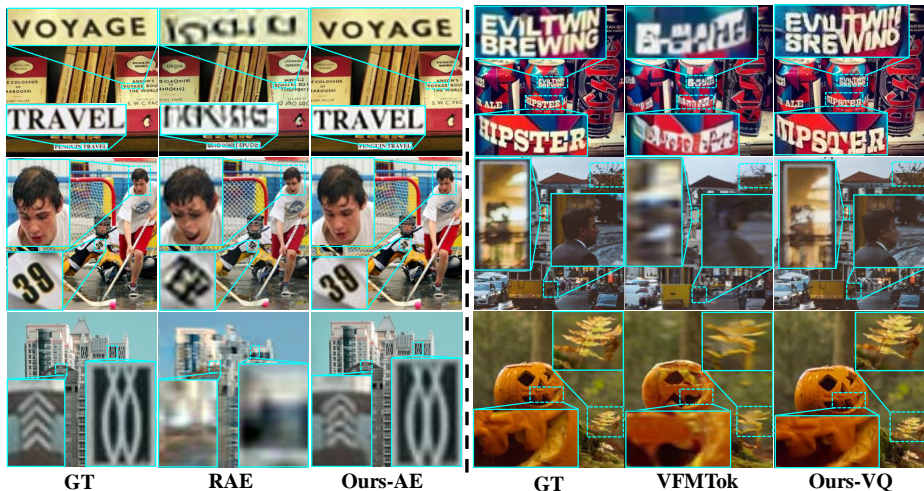


Fig. 6: Qualitative reconstruction results under $16\times$ downsampling. Zoom in for detailed texture comparison. Continuous tokenizers results are shown on the left, and discrete tokenizers on the right. Both DINO-Tok-AE and DINO-Tok-VQ can reconstruct more faithful details and higher-fidelity images compared to the baselines.

(3.08 gFID, 253.6 IS), showing the scaling ability of our DINO-Tok-VQ tokenizer for image generation. Overall, these results demonstrate that DSQ enables high-dimensional, semantics-preserving VQ that remains compatible with strong autoregressive generators, yielding discrete-token models that jointly excel in reconstruction and class-conditional image generation.

Qualitative results. We further visualize reconstruction quality in Fig. 6. Compared to previous tokenizers [13, 59], our approach yields higher fidelity, preserving fine textures and small structures in challenging regions such as faces and embedded text. In contrast, prior methods often produce blurred or distorted content in these areas, or fail to reconstruct them at all, whereas DINO-Tok maintains sharp contours, legible characters, and semantically consistent details.

In Fig. 7, we show class-conditional samples for both continuous- and discrete-space generation, with DINO-Tok-AE on the left and DINO-Tok-VQ on the right. The DINO-Tok-AE generator produces diverse, high-fidelity images with coherent global structure and rich local textures, reflecting the information-complete latent space built from fused semantic and texture features. The DINO-Tok-VQ generator, despite operating on discrete tokens, preserves most of these semantics and fine details, avoiding typical VQ artifacts such as semantic replacement or overly smoothed textures. Across a wide range of classes, both branches exhibit sharp object boundaries, consistent colors, and recognizable fine-grained attributes, confirming that DINO-Tok provides a robust latent interface for both continuous and discrete generative models.



Fig. 7: Class-conditional image generation examples on ImageNet-1k 256×256 . Left: DINO-Tok-AE (continuous latent generation). Right: DINO-Tok-VQ (discrete-token generation). Both branches produce high-quality samples with fine details and broad diversity across different classes.

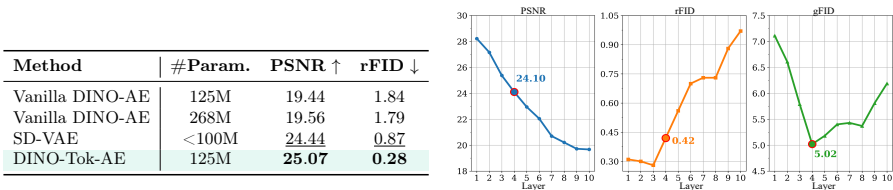


Fig. 8: Left: ImageNet-1k 256×256 reconstructions with varying decoder sizes. Scaling the decoder size yields only marginal improvement. **Right:** Effect of shallow-layer choice on reconstruction and generation, and layer 4 offers the best trade-off.

4.3 Ablation Study

We conduct a comprehensive ablation study on DINO-Tok related to texture feature selection and dominant-subspace quantization. More ablations and analyses are presented in the supplement.

Shallow-layer branch ablation. We study how the choice of the shallow-layer feature affects the texture–semantic trade-off by evaluating reconstruction and generation (40 epochs) results. As shown in Fig. 8 (right) and Fig. 2, earlier layers (e.g., layer 1–3) retain stronger low-level structural signals and thus achieve better rFID and PSNR, but their generative performance (gFID) is weaker. As the shallow branch moves deeper, semantics become stronger and gFID improves, while reconstruction quality consistently degrades. Layer 4 yields the best overall balance, achieving the lowest gFID with competitive rFID and PSNR, indicating that mid-level features provide a good compromise between texture preservation and semantic alignment. We therefore adopt **layer 4** as the default shallow branch in both DINO-Tok-AE and DINO-Tok-VQ.

Table 3: Ablation on Dominant-Subspace Quantization. Quantizing top principal dimensions improves reconstruction and generation, while larger subspaces reduce codebook usage and full 768 dimension quantization collapses.

Type	#Dim	Usage \uparrow	rFID \downarrow	PSNR \uparrow	gFID \downarrow
Top	768	2.3%	–	–	–
Top	64	99.9%	1.44	20.65	<u>8.24</u>
Top	32	100.0%	<u>1.56</u>	<u>20.64</u>	7.25
Random	32	100.0%	2.19	20.16	11.30
Bottom	32	99.9%	6.77	20.42	216.9

Dominant-Subspace Quantization. We further analyze Dominant-Subspace Quantization (DSQ) by varying the semantic subspace dimensionality and the way components are selected, as summarized in Tab. 3. Using all 768 channels for VQ leads to severe codebook collapse (only 2.3% usage) and semantic replacement (see Fig. 4-(B)), which is a clear sign of quantization optimization failure under frozen high-dimensional semantic features. Restricting quantization to the top principal components both stabilizes training and improves performance. Top-64 dimensions give the best reconstruction (1.44 rFID, 20.65 PSNR), while top-32 dimensions achieve the best generative quality (7.25 gFID) with only a minor drop in reconstruction. In contrast, randomly selecting 32 dimensions degrades both rFID and gFID, and quantizing the bottom 32 dimensions causes dramatic failure (gFID \approx 216.9), confirming that low-variance channels contribute little semantic structure and are largely noisy. Based on this trade-off, we use the **top-32 dominant dimensions** as the default semantic subspace in DSQ. Overall, these results support our hypothesis that high-dimensional DINO features exhibit an uneven variance distribution, and that selective quantization over principal components is essential for stable, semantics-preserving VQ.

Decoder Size.

To disentangle representation limitations from decoder capacity, we vary the decoder size while keeping the DINO-base encoder frozen and feeding only the high-level feature \mathbf{F}_{sem} into the decoder which we refer to as **vanilla DINO-AE**. As shown in Fig. 8 (left), scaling the vanilla DINO-AE decoder from 125M to 268M parameters brings only marginal gains (PSNR from 19.44 to 19.56, rFID from 1.84 to 1.79), and both variants remain far behind SD-VAE, whose decoder is even smaller ($<100\text{M}$, 24.44 PSNR, 0.87 rFID). In contrast, with the same 125M decoder budget, DINO-Tok-AE attains 25.07 PSNR and 0.28 rFID by using the information-complete latent. This indicates that the main bottleneck lies in the information content of the latent itself, where high-level DINO features alone lack sufficient high-frequency structure for faithful reconstruction, and simply increasing decoder capacity cannot compensate for this deficiency. The fused multi-layer dual-branch design in DINO-Tok is therefore crucial for unlocking the full potential of frozen DINO representations.

5 Conclusion

In this work, we revisit visual tokenization design through the lens of frozen VFMs and identify two key challenges: the texture–semantic trade-off in reconstruction and the instability of quantizing frozen high-dimensional semantic features. To address these challenges, we introduce DINO-Tok, a unified tokenizer built on DINO that constructs an information-complete latent for continuous tokenization and introduces Dominant-Subspace Quantization (DSQ) to stably discretize principal semantic components. Experiments on ImageNet-1k 256×256 show that DINO-Tok achieves state-of-the-art reconstruction quality and strong continuous- and discrete-space class-conditional generation, demonstrating that frozen VFMs can be directly adapted into high-fidelity, semantically aligned visual tokenizers for next-generation latent generative models.

Appendix

A Ablation on Semantic Similarity Loss

We provide an ablation study on the proposed semantic similarity loss \mathcal{L}_{sem} for DINO-Tok-VQ. The goal of \mathcal{L}_{sem} is to regularize token alignment with the frozen DINO semantics, enhancing semantic structure under DSQ. As shown in Table 4, introducing \mathcal{L}_{sem} consistently improves both reconstruction and generation. In particular, the rFID is reduced from 1.29 to 1.09, while the downstream generation quality is also improved, with gFID decreasing from 4.71 to 3.85 and IS increasing from 212.71 to 237.12. These results indicate that semantic alignment not only benefits representation, but also leads to a more generation-friendly latent space.

Figure 9 further visualizes the effect of \mathcal{L}_{sem} by applying PCA to the latent features. Without \mathcal{L}_{sem} , the latent embeddings already retain coarse semantic structure due to DSQ, but remain noisier and less organized. After introducing \mathcal{L}_{sem} , the embeddings exhibit more compact semantic clusters and clearer structures with reduced noise. This observation is consistent with the quantitative improvements in Table 4, and suggests that \mathcal{L}_{sem} helps preserve more accurate semantic information in the learned tokenizer.

Table 4: Ablation of the semantic similarity loss \mathcal{L}_{sem} on DINO-Tok-VQ for ImageNet-1k 256×256 .

Methods	rFID↓	gFID↓	IS↑
DINO-Tok-VQ w/o \mathcal{L}_{sem}	1.29	4.71	212.71
DINO-Tok-VQ w/ \mathcal{L}_{sem}	1.09	3.85	237.12

B Downstream Linear Probing Evaluation

We further evaluate the semantic quality of different latent representations using linear probing on ImageNet-1k. For all compared methods, the backbone or tokenizer is frozen and only a linear classifier is trained on top of the extracted representation. We follow the standard DINO linear-probing protocol and report the corresponding latent layout for each method (256 tokens for 1D tokenizers and 16×16 for spatial tokenizers). This evaluation complements reconstruction and generation metrics by measuring how much category-level semantic information is preserved in the learned latent space.

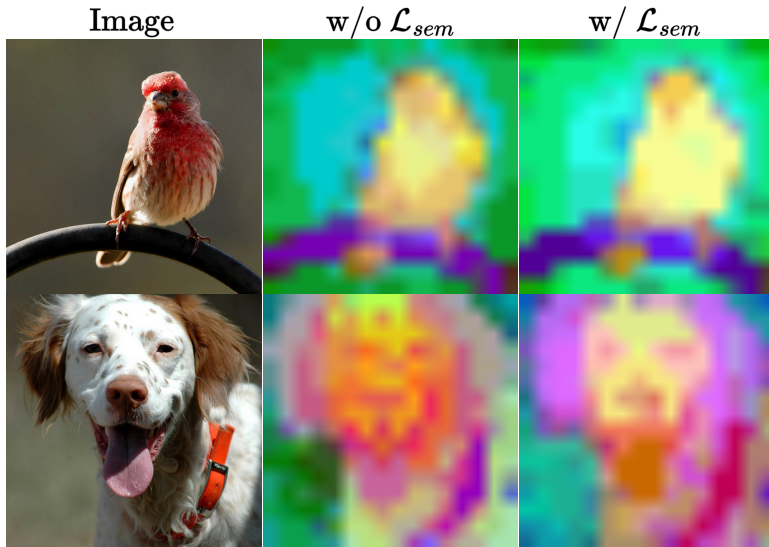


Fig. 9: PCA visualization of latent features with and without the semantic similarity loss \mathcal{L}_{sem} . Introducing \mathcal{L}_{sem} leads to a more organized latent space, with more compact semantic structures and less noise.

The results are summarized in Table 5. Among visual foundation models (VFMs), DINOv3-b achieves the strongest reference performance with 84.9% top-1 accuracy, slightly outperforming DINOv2-b. For discrete tokenizers, DINO-Tok-VQ achieves 77.2% top-1 accuracy, substantially surpassing VFMTok [59], indicating that the proposed DSQ and \mathcal{L}_{sem} preserve stronger dominant semantics. For continuous tokenizers, DINO-Tok-AE reaches 85.0% top-1 accuracy, which is slightly higher than DINOv3-b and also stronger than RAE [60] and SVG [39] in our comparison. We additionally report reconstruction rFID as a reference to show the semantics-texture trade-off. In particular, RAE explicitly uses a frozen pretrained encoder and directly inherits the representation quality of the underlying encoder, while its DINOv2-b-based setting reports 84.5% top-1 accuracy and 0.49 rFID. Compared with this reference, DINO-Tok-AE retains the full semantic representation from the DINO backbone, and further enriches it with an additional shallow-layer branch, achieving a substantially lower rFID of 0.28, suggesting a more favorable balance between semantic preservation and reconstruction fidelity.

C Detailed Reconstruction Results

We report additional reconstruction metrics in Table 6, including LPIPS, PSNR, and SSIM. These metrics complement rFID by measuring perceptual similarity,

Table 5: Linear probing and reconstruction results on ImageNet-1k.

Type	Method	Latent	Acc-Top1↑	rFID↓
VFM	SigLIP-b [44]	16×16	79.1	–
	MAE-b [16]	16×16	68.0	–
	DINOv2-b [31]	16×16	84.5	–
	DINOv3-b [40]	16×16	84.9	–
AE	SD-VAE [13]	16×16	~ 8	0.87
	RAE [60]	16×16	84.5	0.49
	SVG [39]	16×16	79.8	0.65
	Ours-AE	16×16	85.0	0.28

pixel-level fidelity, and structural consistency, respectively. Overall, DINO-Tok demonstrates strong reconstruction quality under both the continuous and discrete settings. For continuous tokenizers, DINO-Tok-AE matches the best reported rFID (0.28) among the compared methods, while also maintaining competitive perceptual and pixel fidelity. Compared with RAE [60] and SVG [39], our method achieves substantially stronger reconstruction quality on pixel-level metrics, indicating that the proposed latent design attains a favorable balance between semantic preservation and image fidelity. Compared with VA-VAE [52], DINO-Tok-AE achieves the same rFID while using a high-dimensional semantic latent space designed to preserve both semantics and reconstruction quality. For discrete tokenizers, DINO-Tok-VQ achieves the best rFID (1.10) among the listed methods, outperforming previous VQ-based and VFM-based tokenizers. Although some baselines achieve slightly stronger LPIPS or PSNR, DINO-Tok-VQ offers a favorable trade-off between semantic preservation, quantization capacity, and reconstruction fidelity, which is also reflected in its stronger downstream linear probing and generation performance.

D Further Analysis of PCA on DINO Features

We present additional PCA-based analyses to better understand the semantic structure of DINO features and to further justify the proposed DSQ strategy. Our observations consistently show that the variance of DINO features is highly concentrated in a small subset of channels, while the remaining channels contribute substantially less. This behavior motivates allocating more modeling or quantization capacity to the principal semantic components.

D.1 Global Consistency of PCA Top Channels

To clarify the motivation of applying DSQ, we examine the global consistency of PCA components across intra-class variations. Specifically, we analyze all 1,300 validation images of the class “ruler” in ImageNet-1k, which exhibit diverse

Table 6: Reconstruction performance on ImageNet-1k 256×256. “ukn.” indicates methods trained with extra datasets or data settings not fully specified in the original source. Despite being trained solely on ImageNet-1k, DINO-Tok achieves strong overall performance across multiple reconstruction metrics.

Type	Method	Dim	Size	rFID ↓	LPIPS ↓	PSNR ↑	SSIM ↑
Continuous	SD-VAE ^{ukn.} [36]	16	-	0.87	0.1363	24.44	0.698
	SVG [39]	392	-	0.65	0.1900	23.89	0.650
	RAE [60]	768	-	0.49	-	19.23	0.620
	VA-VAE [52]	32	-	0.28	0.0962	27.96	0.790
	Ours-AE	832	-	0.28	0.0995	25.07	0.740
Discrete	VQGAN [45]	256	16384	4.98	0.2843	20.00	0.629
	LlamaGen [41]	8	16384	2.19	0.2281	20.79	0.675
	TiTok [54]	16	4096	1.66	-	20.01	-
	Open-MAGVIT2 [27]	18	262144	1.17	0.2038	21.90	-
	VAR [43]	32	4096	-	-	21.30	0.647
	VFMTok [59]	12	16384	1.13	0.2680	19.91	0.488
	IBQ [38]	256	16384	1.37	0.2235	-	-
	Ours-VQ	832	16384 × 2	1.10	0.2382	20.45	0.544

colors, shapes, materials, and backgrounds. As shown in Figure 10, the heatmap demonstrates a strong **global consistency** in channel importance across all instances, with a clear diagonal structure among the top channels. Notably, the top_0 channel (index 755) is activated in 99.8% of all cases (1298/1300). This result indicates that the most dominant PCA channels are not random artifacts, but highly stable semantic directions shared across large appearance variations.

D.2 Channel Shifts Across Different Image Crops

We further investigate the sensitivity of PCA components to semantic changes using different crops from the same image. As shown in Figure 11, crops with distinct semantic emphasis lead to different dominant channels, highlighting the spatial sensitivity of DINO’s representation. The **red** crop, dominated by the eye region, shifts its top principal channel from 755 to 616, indicating a semantic reorientation toward fine-grained details. The **green** crop, which focuses on a local finger region, changes its top channel to 219, reflecting localized texture dominance. By contrast, the **yellow** and **blue** crops, which preserve the ruler and sufficient surrounding context, keep the original dominant channel (755). These observations demonstrate that PCA on DINO features is not only globally consistent, but also sensitive to different semantic contents.

D.3 Long-Tail Distribution of PCA Eigenvalues

We analyze the eigenvalue spectrum of PCA applied to DINO features to understand how variance is distributed across channels. As illustrated in Figure 12,

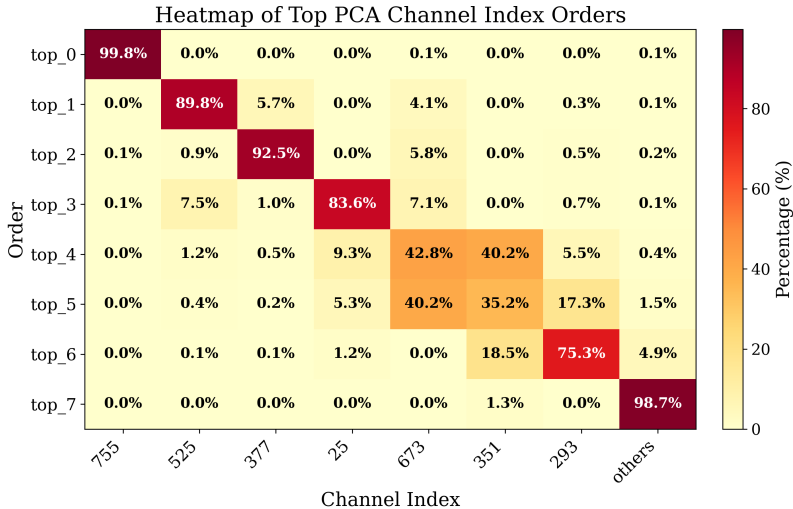


Fig. 10: PCA on DINO features for all “ruler” images in ImageNet reveals globally consistent channel importance. The top channels are highly consistent across diverse instances, and the top_0 channel (index 755) is activated in 99.8% of all cases.

the eigenvalue distribution follows a clear long-tail pattern, indicating that only a small number of principal components account for the majority of the representational variance. This concentration suggests that semantic information is unevenly distributed in the feature space, providing direct motivation for extracting dominant subspaces during quantization.

D.4 Complete DINO Sorted Channels Visualization

We provide a complete visualization of all 768 PCA-sorted channels from DINO-v3-base and DINO-v2-base in Figure 13 and Figure 14. The top channels show clear semantic structures and object-aligned patterns, while the bottom channels become increasingly noisy and difficult to interpret. This progressive transition from structured to noisy channels further supports the dominant-subspace assumption used in our quantization design.

E Theoretical Analysis of the Distance Concentration Phenomenon

We provide a brief theoretical background on why Euclidean (L_2) distance-based lookup in traditional vector quantization becomes unreliable in high-dimensional spaces. As shown in prior work [2, 6, 33], the distance concentration behavior of

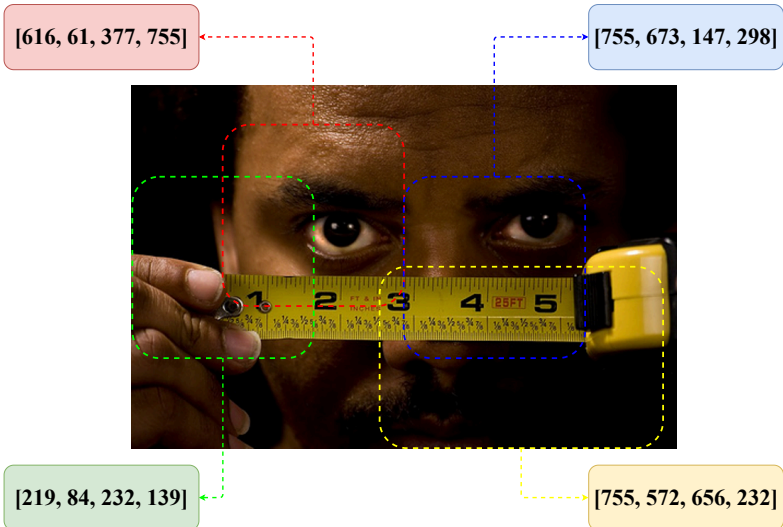


Fig. 11: PCA of DINO embeddings under different image crops. Different crops induce different dominant channels, showing that the leading PCA components are sensitive to semantic content and local structures.

Minkowski distances is a direct consequence of concentration-of-measure phenomena in high dimensions.

Consider a set of n data points $\mathcal{P} = \{\mathbf{P}_1^d, \dots, \mathbf{P}_n^d\}$, where each point $\mathbf{P}_i^d = (p_i^1, \dots, p_i^d) \in \mathbb{R}^d$, and a query point $\mathbf{Q}^d = (q^1, \dots, q^d) \in \mathbb{R}^d$. The p -norm (Minkowski) distance between \mathbf{P}_i^d and \mathbf{Q}^d is defined as

$$L_p(\mathbf{P}_i^d, \mathbf{Q}^d) = \left(\sum_{k=1}^d |p_i^k - q^k|^p \right)^{1/p}, \quad (4)$$

which reduces to the standard Euclidean distance when $p = 2$.

Formally, as the dimensionality d grows, the relative contrast between the farthest and nearest samples vanishes:

$$\lim_{d \rightarrow \infty} \frac{D_{\max}^d - D_{\min}^d}{D_{\min}^d} = 0, \quad (5)$$

where

$$\begin{aligned} D_{\max}^d &= \max_{i=1, \dots, n} \|\mathbf{P}_i^d - \mathbf{Q}^d\|_p, \\ D_{\min}^d &= \min_{i=1, \dots, n} \|\mathbf{P}_i^d - \mathbf{Q}^d\|_p. \end{aligned} \quad (6)$$

In other words, nearest and farthest neighbors become increasingly indistinguishable in high dimensions. For high-dimensional visual tokens, this phenomenon

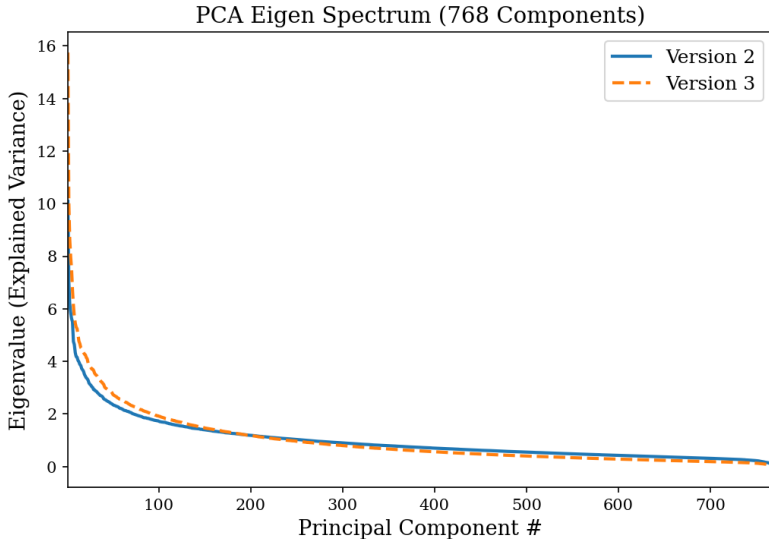


Fig. 12: PCA eigenvalue distribution of DINO-v2 and DINO-v3 features. The long-tail spectrum indicates that only a few dominant channels capture most of the representational variance.

weakens the effectiveness of plain L_2 lookup and motivates our DSQ strategy, which emphasizes dominant semantic channels rather than treating all channels uniformly.

F More Qualitative Visualizations

We provide additional qualitative visualizations of generation and reconstruction in Figure 15 and Figure 16. DINO-Tok-AE and DINO-Tok-VQ produces diverse and visually plausible class-conditional samples with fine local details. Figures 17 and 18 further show that both DINO-Tok-AE and DINO-Tok-VQ reconstruct faithful image structures, object boundaries, and fine textures.

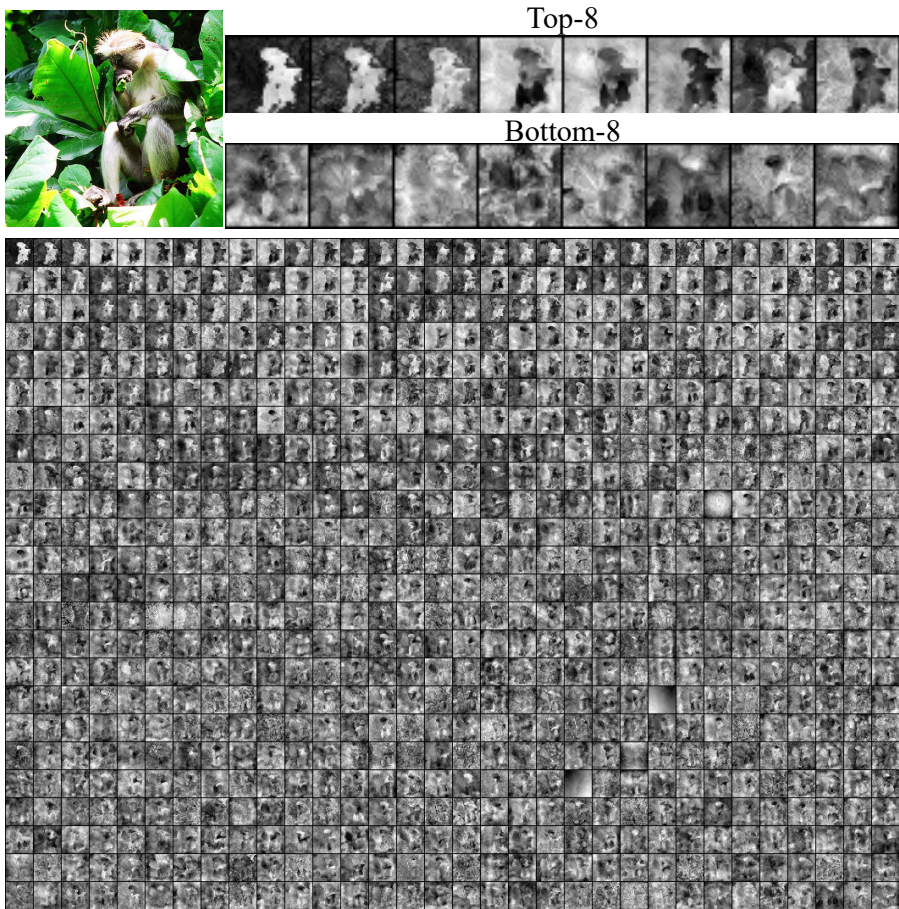


Fig. 13: Visualization of all PCA-sorted 768 channels of DINO-v3-base features. Channels are ordered by PCA importance. Top channels exhibit clear semantic structure, while bottom channels appear increasingly noisy.

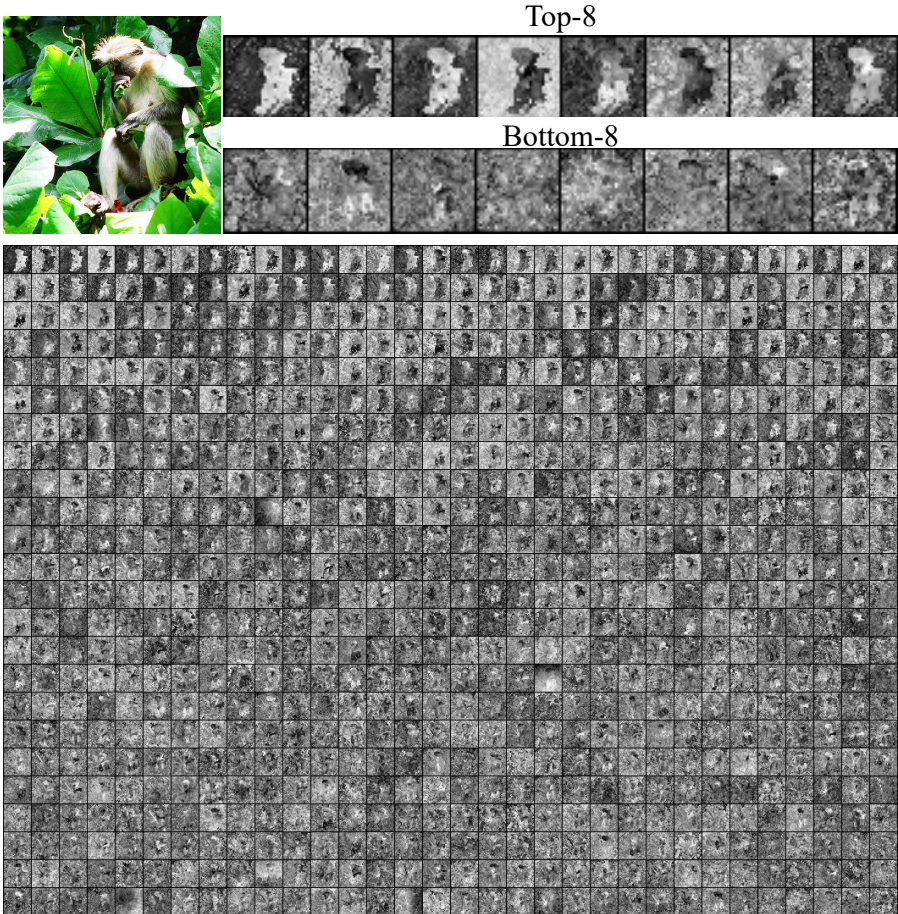


Fig. 14: Visualization of all PCA-sorted 768 channels of DINO-v2-base features. Similar to DINO-v3-base, the most dominant channels are much more interpretable than the low-ranked channels.

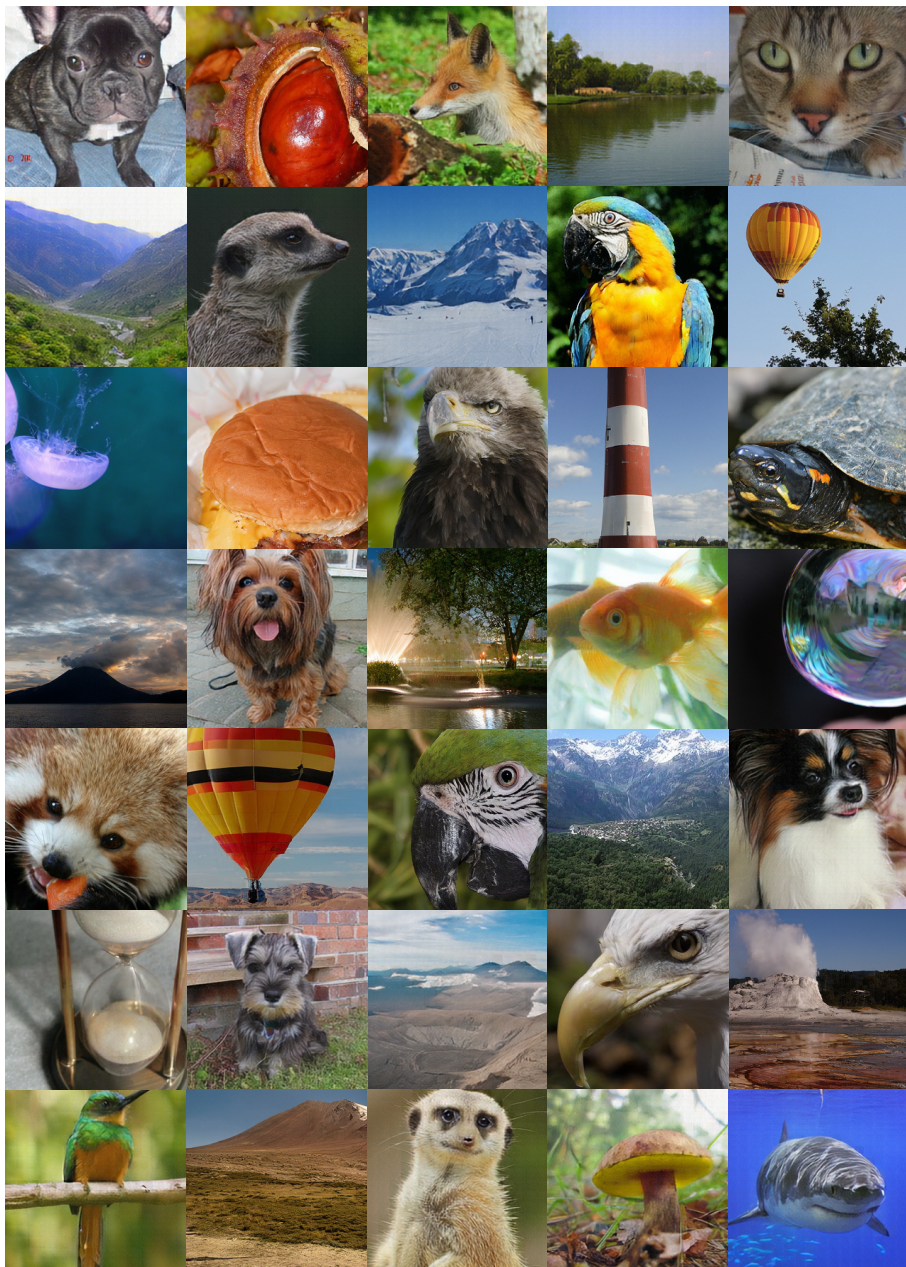


Fig. 15: More qualitative image generation results of DINO-Tok-AE. DINO-Tok-AE produces high-quality and diverse class-conditional generations across different semantic categories.



Fig. 16: More qualitative image generation results of DINO-Tok-VQ. DINO-Tok-VQ produces high-quality and diverse class-conditional generations across different semantic categories.



Fig. 17: More qualitative results of continuous tokenizer reconstruction. DINO-Tok can reconstruct more faithful details and higher-fidelity images compared to the baseline.



Fig. 18: More qualitative results of discrete tokenizer reconstruction. DINO-Tok can reconstruct more faithful details and higher-fidelity images compared to the baseline.

References

1. Agarwal, N., Ali, A., Bala, M., Balaji, Y., Barker, E., Cai, T., Chattopadhyay, P., Chen, Y., Cui, Y., Ding, Y., et al.: Cosmos world foundation model platform for physical ai. arXiv preprint arXiv:2501.03575 (2025)
2. Aggarwal, C.C., Hinneburg, A., Keim, D.A.: On the surprising behavior of distance metrics in high dimensional space. In: International conference on database theory. pp. 420–434. Springer (2001)
3. Bachmann, R., Allardice, J., Mizrahi, D., Fini, E., Kar, O.F., Amirloo, E., El-Nouby, A., Zamir, A., Dehghan, A.: Flextok: Resampling images into 1d token sequences of flexible length. In: Forty-second International Conference on Machine Learning (2025)
4. Bai, J., Bai, S., Yang, S., Wang, S., Tan, S., Wang, P., Lin, J., Zhou, C., Zhou, J.: Qwen-vl: A frontier large vision-language model with versatile abilities. arXiv preprint arXiv:2308.12966 1(2), 3 (2023)
5. Bai, Z., Gao, J., Gao, Z., Wang, P., Zhang, Z., He, T., Shou, M.Z.: Factorized visual tokenization and generation. arXiv preprint arXiv:2411.16681 (2024)
6. Beyer, K., Goldstein, J., Ramakrishnan, R., Shaft, U.: When is “nearest neighbor” meaningful? In: International conference on database theory. pp. 217–235. Springer (1999)
7. Caron, M., Touvron, H., Misra, I., Jégou, H., Mairal, J., Bojanowski, P., Joulin, A.: Emerging properties in self-supervised vision transformers. In: Proceedings of the IEEE/CVF international conference on computer vision. pp. 9650–9660 (2021)
8. Chang, H., Zhang, H., Jiang, L., Liu, C., Freeman, W.T.: Maskgit: Masked generative image transformer. In: Proceedings of the IEEE/CVF conference on computer vision and pattern recognition. pp. 11315–11325 (2022)
9. Chen, L., Li, Z., Lin, B., Zhu, B., Wang, Q., Yuan, S., Zhou, X., Cheng, X., Yuan, L.: Od-vae: An omni-dimensional video compressor for improving latent video diffusion model. arXiv preprint arXiv:2409.01199 (2024)
10. Dai, X., Hou, J., Ma, C.Y., Tsai, S., Wang, J., Wang, R., Zhang, P., Vandenhende, S., Wang, X., Dubey, A., et al.: Emu: Enhancing image generation models using photogenic needles in a haystack. arXiv preprint arXiv:2309.15807 (2023)
11. Deng, J., Dong, W., Socher, R., Li, L.J., Li, K., Fei-Fei, L.: Imagenet: A large-scale hierarchical image database. In: CVPR. pp. 248–255. Ieee (2009)
12. Esser, P., Kulal, S., Blattmann, A., Entezari, R., Müller, J., Saini, H., Levi, Y., Lorenz, D., Sauer, A., Boesel, F., et al.: Scaling rectified flow transformers for high-resolution image synthesis. In: Forty-first international conference on machine learning (2024)
13. Esser, P., Kulal, S., Blattmann, A., Entezari, R., Müller, J., Saini, H., Levi, Y., Lorenz, D., Sauer, A., Boesel, F., et al.: Scaling rectified flow transformers for high-resolution image synthesis. In: ICML (2024)
14. Esser, P., Rombach, R., Ommer, B.: Taming transformers for high-resolution image synthesis. In: Proceedings of the IEEE/CVF conference on computer vision and pattern recognition. pp. 12873–12883 (2021)
15. Gao, S., Zhou, P., Cheng, M.M., Yan, S.: Masked diffusion transformer is a strong image synthesizer. In: Proceedings of the IEEE/CVF international conference on computer vision. pp. 23164–23173 (2023)
16. He, K., Chen, X., Xie, S., Li, Y., Dollár, P., Girshick, R.: Masked autoencoders are scalable vision learners. In: Proceedings of the IEEE/CVF conference on computer vision and pattern recognition. pp. 16000–16009 (2022)

17. Hu, X., Yin, W., Jia, M., Deng, J., Guo, X., Zhang, Q., Long, X., Tan, P.: Drivingworld: Constructing world model for autonomous driving via video gpt. arXiv preprint arXiv:2412.19505 (2024)
18. Jia, M., Yin, W., Hu, X., Guo, J., Guo, X., Zhang, Q., Long, X.X., Tan, P.: Mgvq: Could vq-vae beat vae? a generalizable tokenizer with multi-group quantization. arXiv preprint arXiv:2507.07997 (2025)
19. Kingma, D.P., Welling, M.: Auto-encoding variational bayes. arXiv preprint arXiv:1312.6114 (2013)
20. Kirillov, A., Mintun, E., Ravi, N., Mao, H., Rolland, C., Gustafson, L., Xiao, T., Whitehead, S., Berg, A.C., Lo, W.Y., et al.: Segment anything. In: Proceedings of the IEEE/CVF international conference on computer vision. pp. 4015–4026 (2023)
21. Kong, L., Yang, W., Mei, J., Liu, Y., Liang, A., Zhu, D., Lu, D., Yin, W., Hu, X., Jia, M., et al.: 3d and 4d world modeling: A survey. arXiv preprint arXiv:2509.07996 (2025)
22. Lee, D., Kim, C., Kim, S., Cho, M., Han, W.S.: Autoregressive image generation using residual quantization. In: Proceedings of the IEEE/CVF conference on computer vision and pattern recognition. pp. 11523–11532 (2022)
23. Li, J., Li, D., Savarese, S., Hoi, S.: Blip-2: Bootstrapping language-image pre-training with frozen image encoders and large language models. In: International conference on machine learning. pp. 19730–19742. PMLR (2023)
24. Li, X., Qiu, K., Chen, H., Kuen, J., Gu, J., Raj, B., Lin, Z.: Imagefolder: Autoregressive image generation with folded tokens. arXiv preprint arXiv:2410.01756 (2024)
25. Li, Z., Liu, X., Zhang, X., Tan, P., Shum, H.Y.: Noisear: Autoregressing initial noise prior for diffusion models. arXiv preprint arXiv:2506.01337 (2025)
26. Loshchilov, I., Hutter, F.: Decoupled weight decay regularization. arXiv preprint arXiv:1711.05101 (2017)
27. Luo, Z., Shi, F., Ge, Y., Yang, Y., Wang, L., Shan, Y.: Open-magvit2: An open-source project toward democratizing auto-regressive visual generation. arXiv preprint arXiv:2409.04410 (2024)
28. Ma, C., Jiang, Y., Wu, J., Yang, J., Yu, X., Yuan, Z., Peng, B., Qi, X.: Uniktok: A unified tokenizer for visual generation and understanding. arXiv preprint arXiv:2502.20321 (2025)
29. Ma, N., Goldstein, M., Albergo, M.S., Boffi, N.M., Vanden-Eijnden, E., Xie, S.: Sit: Exploring flow and diffusion-based generative models with scalable interpolant transformers. In: European Conference on Computer Vision. pp. 23–40. Springer (2024)
30. Mentzer, F., Minnen, D., Agustsson, E., Tschannen, M.: Finite scalar quantization: Vq-vae made simple. arXiv preprint arXiv:2309.15505 (2023)
31. Oquab, M., Darcet, T., Moutakanni, T., Vo, H., Szafraniec, M., Khalidov, V., Fernandez, P., Haziza, D., Massa, F., El-Nouby, A., et al.: Dinov2: Learning robust visual features without supervision. arXiv preprint arXiv:2304.07193 (2023)
32. Peebles, W., Xie, S.: Scalable diffusion models with transformers. In: Proceedings of the IEEE/CVF international conference on computer vision. pp. 4195–4205 (2023)
33. Peng, D., Gui, Z., Wu, H.: Interpreting the curse of dimensionality from distance concentration and manifold effect. arXiv preprint arXiv:2401.00422 (2023)
34. Radford, A., Kim, J.W., Hallacy, C., Ramesh, A., Goh, G., Agarwal, S., Sastry, G., Askell, A., Mishkin, P., Clark, J., et al.: Learning transferable visual models from natural language supervision. In: International conference on machine learning. pp. 8748–8763. PmLR (2021)

35. Ramesh, A., Pavlov, M., Goh, G., Gray, S., Voss, C., Radford, A., Chen, M., Sutskever, I.: Zero-shot text-to-image generation. In: International conference on machine learning. pp. 8821–8831. Pmlr (2021)
36. Rombach, R., Blattmann, A., Lorenz, D., Esser, P., Ommer, B.: High-resolution image synthesis with latent diffusion models. In: Proceedings of the IEEE/CVF conference on computer vision and pattern recognition. pp. 10684–10695 (2022)
37. Sargent, K., Hsu, K., Johnson, J., Fei-Fei, L., Wu, J.: Flow to the mode: Mode-seeking diffusion autoencoders for state-of-the-art image tokenization. In: Proceedings of the IEEE/CVF International Conference on Computer Vision. pp. 19471–19481 (2025)
38. Shi, F., Luo, Z., Ge, Y., Yang, Y., Shan, Y., Wang, L.: Scalable image tokenization with index backpropagation quantization. In: Proceedings of the IEEE/CVF International Conference on Computer Vision. pp. 16037–16046 (2025)
39. Shi, M., Wang, H., Zheng, W., Yuan, Z., Wu, X., Wang, X., Wan, P., Zhou, J., Lu, J.: Latent diffusion model without variational autoencoder. arXiv preprint arXiv:2510.15301 (2025)
40. Siméoni, O., Vo, H.V., Seitzer, M., Baldassarre, F., Oquab, M., Jose, C., Khali-dov, V., Szafraniec, M., Yi, S., Ramamonjisoa, M., et al.: Dinov3. arXiv preprint arXiv:2508.10104 (2025)
41. Sun, P., Jiang, Y., Chen, S., Zhang, S., Peng, B., Luo, P., Yuan, Z.: Autoregressive model beats diffusion: Llama for scalable image generation. arXiv preprint arXiv:2406.06525 (2024)
42. Tan, Z., Xue, B., Jia, J., Wang, J., Ye, W., Shi, S., Sun, M., Wu, W., Chen, Q., Jiang, P.: Sweettok: Semantic-aware spatial-temporal tokenizer for compact video discretization. In: Proceedings of the IEEE/CVF International Conference on Computer Vision. pp. 23541–23550 (2025)
43. Tian, K., Jiang, Y., Yuan, Z., Peng, B., Wang, L.: Visual autoregressive modeling: Scalable image generation via next-scale prediction. NeurIPS **37**, 84839–84865 (2025)
44. Tschannen, M., Gritsenko, A., Wang, X., Naeem, M.F., Alabdulmohsin, I., Parthasarathy, N., Evans, T., Beyer, L., Xia, Y., Mustafa, B., et al.: Siglip 2: Multilingual vision-language encoders with improved semantic understanding, localization, and dense features. arXiv preprint arXiv:2502.14786 (2025)
45. Van Den Oord, A., Vinyals, O., et al.: Neural discrete representation learning. *Advances in neural information processing systems* **30** (2017)
46. Wang, J., Jiang, Y., Yuan, Z., Peng, B., Wu, Z., Jiang, Y.G.: Omnitokenizer: A joint image-video tokenizer for visual generation. *Advances in Neural Information Processing Systems* **37**, 28281–28295 (2024)
47. Wang, X., Zhang, X., Luo, Z., Sun, Q., Cui, Y., Wang, J., Zhang, F., Wang, Y., Li, Z., Yu, Q., et al.: Emu3: Next-token prediction is all you need. arXiv preprint arXiv:2409.18869 (2024)
48. Wu, P., Zhu, K., Liu, Y., Tang, L., Yang, J., Peng, Y., Zhai, W., Cao, Y., Zha, Z.J.: Alitok: Towards sequence modeling alignment between tokenizer and autoregressive model. arXiv preprint arXiv:2506.05289 (2025)
49. Xie, J., Mao, W., Bai, Z., Zhang, D.J., Wang, W., Lin, K.Q., Gu, Y., Chen, Z., Yang, Z., Shou, M.Z.: Show-o: One single transformer to unify multimodal understanding and generation. arXiv preprint arXiv:2408.12528 (2024)
50. Xiong, T., Liew, J.H., Huang, Z., Feng, J., Liu, X.: Gigatok: Scaling visual tokenizers to 3 billion parameters for autoregressive image generation. arXiv preprint arXiv:2504.08736 (2025)

51. Yao, J., Wang, C., Liu, W., Wang, X.: Fasterdit: Towards faster diffusion transformers training without architecture modification. *Advances in Neural Information Processing Systems* **37**, 56166–56189 (2024)
52. Yao, J., Yang, B., Wang, X.: Reconstruction vs. generation: Taming optimization dilemma in latent diffusion models. In: *Proceedings of the Computer Vision and Pattern Recognition Conference*. pp. 15703–15712 (2025)
53. Yu, L., Lezama, J., Gundavarapu, N.B., Versari, L., Sohn, K., Minnen, D., Cheng, Y., Birodkar, V., Gupta, A., Gu, X., et al.: Language model beats diffusion-tokenizer is key to visual generation. *arXiv preprint arXiv:2310.05737* (2023)
54. Yu, Q., Weber, M., Deng, X., Shen, X., Cremers, D., Chen, L.C.: An image is worth 32 tokens for reconstruction and generation. *Advances in Neural Information Processing Systems* **37**, 128940–128966 (2024)
55. Yu, S., Kwak, S., Jang, H., Jeong, J., Huang, J., Shin, J., Xie, S.: Representation alignment for generation: Training diffusion transformers is easier than you think. *arXiv preprint arXiv:2410.06940* (2024)
56. Zhang, B., Rao, Q., Zheng, W., Zhou, J., Lu, J.: Quantize-then-rectify: Efficient vq-vae training. *arXiv preprint arXiv:2507.10547* (2025)
57. Zhao, S., Zhang, Y., Cun, X., Yang, S., Niu, M., Li, X., Hu, W., Shan, Y.: Cv-vae: A compatible video vae for latent generative video models. *Advances in Neural Information Processing Systems* **37**, 12847–12871 (2024)
58. Zhao, Y., Xiong, Y., Krähenbühl, P.: Image and video tokenization with binary spherical quantization. *arXiv preprint arXiv:2406.07548* (2024)
59. Zheng, A., Wen, X., Zhang, X., Ma, C., Wang, T., Yu, G., Zhang, X., Qi, X.: Vision foundation models as effective visual tokenizers for autoregressive image generation. *arXiv preprint arXiv:2507.08441* (2025)
60. Zheng, B., Ma, N., Tong, S., Xie, S.: Diffusion transformers with representation autoencoders. *arXiv preprint arXiv:2510.11690* (2025)
61. Zheng, H., Nie, W., Vahdat, A., Anandkumar, A.: Fast training of diffusion models with masked transformers. *arXiv preprint arXiv:2306.09305* (2023)
62. Zhu, L., Wei, F., Lu, Y., Chen, D.: Scaling the codebook size of vq-gan to 100,000 with a utilization rate of 99%. *Advances in Neural Information Processing Systems* **37**, 12612–12635 (2024)
63. Zhu, Y., Li, B., Xin, Y., Xia, Z., Xu, L.: Addressing representation collapse in vector quantized models with one linear layer. In: *Proceedings of the IEEE/CVF International Conference on Computer Vision*. pp. 22968–22977 (2025)
64. Zhuang, S., Guo, Y., Fu, C., Huang, Z., Tian, Z., Wang, F., Zhang, Y., Li, C., Wang, Y.: Wetok: Powerful discrete tokenization for high-fidelity visual reconstruction. *arXiv preprint arXiv:2508.05599* (2025)